Uncertainty quantification simulation of the HyShot II flight experiment

By J. A. S. Witteveen AND G. Iaccarino

1. Motivation and objectives

The numerical prediction of scramjet in-flight performance is a landmark example in which current simulation capability is overwhelmed by abundant uncertainty and error. The objective of the Predictive Science Academic Alliance Program (PSAAP) at Stanford University is to improve this predictive capability for the design of future scramjet engines in hypersonic flight systems. We define a predictive simulation as a numerical computation in which the effects of uncertainty and error on the output quantity of interest (QOI) are sufficiently reduced to use the results for design purposes. The computational focus of the Stanford PSAAP team (Pečnik *et al.* 2009; Wang *et al.* 2010) is the validation of state-of-the-art modeling codes for the HyShot II scramjet flight experiment (Smart *et al.* 2006) performed by the University of Queensland in Australia (see Figure 1a).

The sketch of the quantification of margins and uncertainties (QMU) diagram of the HyShot II performance, depicted in Figure 1b, shows the variation of the thrust between the critical *no thrust* and *unstart* boundaries as a function of the fuel injection rate in time. Current numerical predictions are hampered by limited accuracy, and this is represented in terms of the wide probability density function (PDF) at the right of the figure, which shows too large a spread beyond the operability limits for the simulation results to be useful in the design process. The uncertainties therefore need to be reduced until their effect is sufficiently small compared to the design margins, as shown by the PDF with smaller variance in Figure 1b. The objective of this work is to develop a decision-making framework for systematically balancing and reducing uncertainties and errors. The proposed tool is applied to the simulation of the HyShot II flight experiment.

Uncertainty quantification (UQ) is an essential part of the QMU process, which is concerned with the computation of the impact of different sources of uncertainty on the QOI. Aleatoric uncertainties, or irreducible uncertainties, describe physical variations caused by intrinsic randomness in the system or its environment (Oberkampf *et al.* 2004). These uncertainties can be characterized in terms of probability distributions and covariance matrices. Epistemic uncertainty is a second type of uncertainty caused by a certain lack of knowledge, which is not probabilistic in nature. The lack of knowledge can result from structural uncertainty in the model form or insufficient measurement data to quantify the value of an input parameter. An essential property of epistemic uncertainties is that they can be reduced either by increasing model fidelity or by performing additional experiments.

Uncertainty quantification methods for both types of uncertainties are, therefore, necessary in the QMU process. Quantification of the effect of aleatoric input uncertainties requires their propagation through a computational model using probabilistic methods. Polynomial Chaos (Ghanem & Spanos 1991; Xiu & Karniadakis 2002) (PC) and Stochastic Collocation (Babuška *et al.* 2007; Xiu & Hesthaven 2005) (SC) approaches are widely

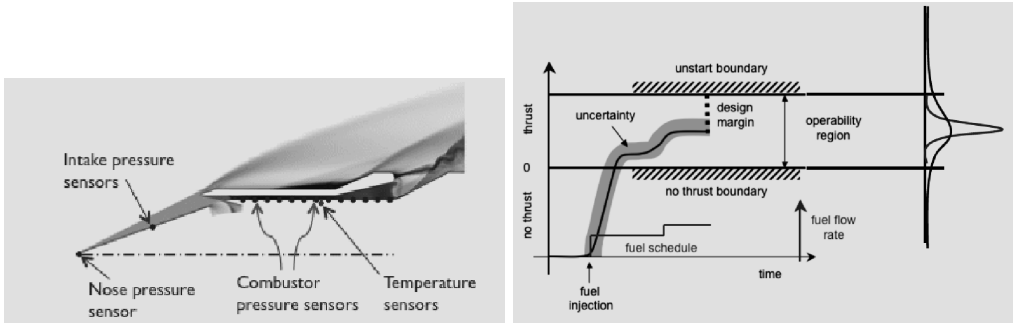

(a) HyShot II scramjet engine (b) Performance margins and uncertainties

FIGURE 1. Quantification of margins and uncertainties (QMU) schematics for the HyShot II flight experiment validation.

used for aleatoric uncertainty propagation. The non-intrusive SC method is preferred in large-scale computational problems since it is based on a series of deterministic simulations for sampled values of the aleatoric parameters. However, these methods can be ineffective in treating correlated inputs, non-standard distributions, and discontinuous responses. In contrast, there is no consensus on the general mathematical description of epistemic uncertainties. Quantification of epistemic uncertainty is, therefore, also an unresolved issue, and an active field of research (Jakeman *et al.* 2010; Tang *et al.* 2010). Computer simulations are also inherently subjected to numerical errors, such as mesh and time-step discretization errors, iteration errors in nonlinear problems, and computer round-off errors. The proposed framework for balancing uncertainties and errors incorporates these separate methods for aleatoric and epistemic uncertainty quantification and for numerical error estimation.

The uncertainty quantification simulation of the HyShot II flight experiment is detailed in Section 3. First, the framework for balancing uncertainties and errors is introduced in Section 2. In Section 4, the numerical results are presented for the non-reactive HyShot II case with aleatoric and epistemic uncertainty. The paper concludes with a discussion of future plans in Section 5.

2. Balancing uncertainties and errors

In order to take into account the effect of all uncertainties and errors, a deterministic simulation is not sufficient because one needs to propagate aleatoric uncertainty, quantify epistemic uncertainty, and estimate numerical errors, as shown in Figure 2a. The decision-making tool then uses these inputs to indicate whether to invest additional resources in either more aleatoric uncertainty sampling, model fidelity improvement, or spatial mesh refinement to reduce the aleatoric uncertainty propagation error, epistemic uncertainty, or numerical error, respectively. Model fidelity and discretization error are here used as examples of epistemic uncertainty and numerical error, respectively.

Balancing the computational efforts in the three types of uncertainty and error is, therefore, equivalent to balancing the aleatoric uncertainty propagation error, the epistemic uncertainty, and the numerical error. The present methodology is based on a non-intrusive approach to propagate aleatory uncertainty in which the aleatoric output uncertainty is computed by analyzing the results of multiple deterministic simulations for varying aleatoric parameter values in an aleatoric post-processing step. For the samples

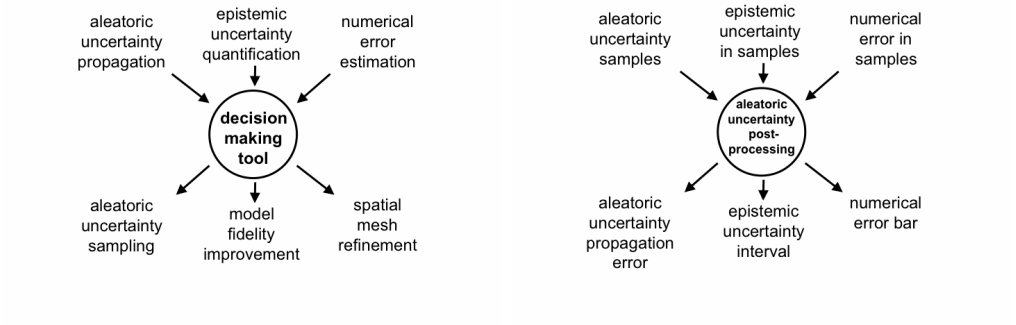

(a) Balancing resources (b) Balancing uncertainties and errors

FIGURE 2. Balancing aleatoric, epistemic, and numerical efforts.

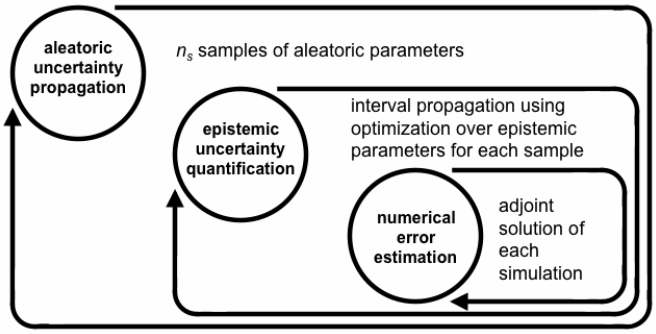

FIGURE 3. Nested uncertainty quantification and error estimation loop.

an evaluation of the epistemic uncertainty and the discretization error is also computed. The post-processing step is, therefore, the most suitable component of the UQ process in which to perform this decision making, since the aleatoric uncertainty samples are inputs to this post-processing as well as the epistemic uncertainty and the numerical error in these samples, see Figure 2b. The aleatoric post-processing is then in the position to compute the combined effect of the aleatoric uncertainty propagation error, the epistemic uncertainty interval, and the numerical error bar on the probabilistic output for the QOI.

An important component of the balancing process is the nested uncertainty quantification and error estimation loop shown in Figure 3. For aleatoric uncertainty propagation, n_s samples are drawn in the space of the aleatoric input parameters. The location of the sampling points depends on the aleatoric uncertainty quantification method used. In order to compute the effect of epistemic uncertainty, an epistemic uncertainty quantification is performed for each aleatoric sample. One approach to quantify epistemic uncertainty is to propagate an epistemic input interval to the output using optimization over the space of the epistemic parameters to find the minimum and maximum of the output interval. The contribution of spatial discretization to the numerical error can be estimated by solving, for example, an adjoint problem for each simulation performed in the epistemic optimization loop.

Recombining numerical error estimation with epistemic uncertainty quantification and aleatoric uncertainty propagation yields an estimate of the impact of all sources of un-

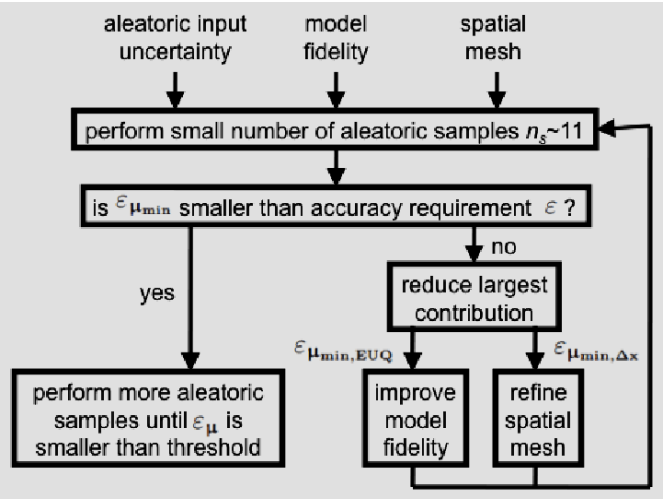

FIGURE 4. Uncertainty quantification and error estimation decision-making framework.

certainty and error on the QOI. The result is then a cumulative probability distribution function (CDF) superimposed by a confidence interval that accounts for the aleatoric uncertainty propagation error, the epistemic uncertainty, and the numerical error. As a consequence, confidence intervals for the statistical moments and the percentiles are obtained.

The framework for balancing uncertainties and errors is presented in the form of a block diagram in Figure 4. At the start of the process the aleatoric input uncertainty is characterized and quantified. An initial model fidelity and spatial discretization are also selected. This initial numerical description can be based on a low-fidelity model and a coarse mesh.

The first step is then to perform the smallest number of aleatoric samples, in the sense of Figure 3, necessary to estimate the aleatoric uncertainty propagation error, for example, for the mean ε_μ. This includes an estimate of the minimum error $\varepsilon_{\mu_{\min}}$ that can be obtained by increasing the number of aleatoric samples n_s. This residual error $\varepsilon_{\mu_{\min}}$ is caused by the contribution of epistemic uncertainty and numerical error. If the estimate of the minimum obtainable error $\varepsilon_{\mu_{\min}}$ is smaller than an accuracy requirement ε, then the aleatoric sampling loop of Figure 3 is performed until ε_μ reaches the threshold. The minimum error estimate $\varepsilon_{\mu_{\min}}$ can change slightly with increasing numbers of samples. Therefore, $\varepsilon_{\mu_{\min}}$ has to be smaller than ε with some margin to avoid $\varepsilon_{\mu_{\min}}$ becoming larger than ε after adding more samples. Otherwise, the process has to be restarted by performing the initial aleatoric samples again with a higher-fidelity model or a finer mesh.

On the other hand, if $\varepsilon_{\mu_{\min}}$ is larger than the threshold ε, then the separate contributions of the epistemic uncertainty $\varepsilon_{\mu_{\min,\mathrm{EUQ}}}$ and the numerical error $\varepsilon_{\mu_{\min,\Delta x}}$ to $\varepsilon_{\mu_{\min}}$ are compared. In order to reduce the largest contribution, either the model fidelity needs to be improved or the spatial mesh refined. The new model or discretization is used to repeat the computations for the initial aleatoric samples. The resulting $\varepsilon_{\mu_{\min}}$ is then compared to the threshold ε, and so on until $\varepsilon_{\mu_{\min}}$ is small enough. This process leads to a *validation simulation* analogous to a validation experiment, where all sources of uncertainty and error are taken into account and efficiently reduced below a tolerance ε.

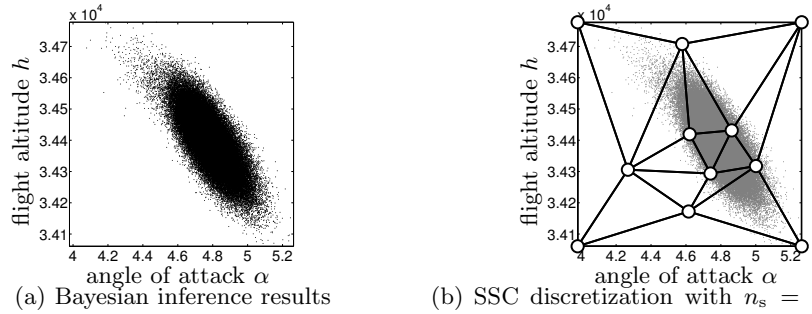

(a) Bayesian inference results

(b) SSC discretization with $n_s = 11$ samples denoted by circles

FIGURE 5. Probability distribution of the aleatoric angle of attack and the flight altitude for the HyShot II flight experiment.

It can eventually also result in the conclusion that the confidence requirement ε cannot be met within the available computational budget.

To minimize the number of cycles in the process, it is important to determine the improvement of model fidelity or spatial mesh refinement required in each step. Based on the order of convergence of the spatial discretization, the required mesh size can be estimated. In contrast, the reduction of epistemic uncertainty resulting from an improvement in model fidelity is more difficult to predict. Finding a higher fidelity model also requires detailed insight into the relevant physical processes, which makes it a highly problem-dependent step.

3. Application to the HyShot II flight experiment

The presented framework is applied to the HyShot II flight experiment starting with the propagation of aleatoric uncertainty using the Simplex Stochastic Collocation (SSC) method (Witteveen & Iaccarino 2010*b*).

3.1. *Aleatoric flight conditions*

The flow conditions of the HyShot II flight are somewhat uncertain due to the failure of the radar tracking system during the experiment. Therefore, the free stream conditions were inferred from pressure measurements in the unfueled side of the combustor in a previous study using Bayesian inversion (Constantine *et al.* 2010). The result of the Bayesian inference analysis is shown in Figure 5a for the angle of attack α and flight altitude h for test case 2 at t=538.172s from Smart *et al.* (2006). The probability distribution of the flow conditions shows a highly correlated structure with a coefficient of variation (CV) of 2.1% for the angle of attack and 0.2% for flight altitude. This variability also includes uncertainty caused by the pressure measurements and the ill-posedness of the inverse problem. In this case the Mach number is kept constant at 7.831.

The flight conditions can be considered to be aleatoric uncertainties, in the sense that they are described by a probability distribution and a correlation. The distribution that follows from Bayesian inverse analysis is given by the set of Markov Chain Monte Carlo (MCMC) data points shown in Figure 5a. Currently available aleatoric uncertainty quantification methods are, however, usually based on assumptions of uncorrelated inputs and standard distributions in functional form. This holds, for example, for the widely used Stochastic Collocation method, which uses Gauss quadrature sampling and global Lagrangian polynomial interpolation in probability space. However, both assumptions are

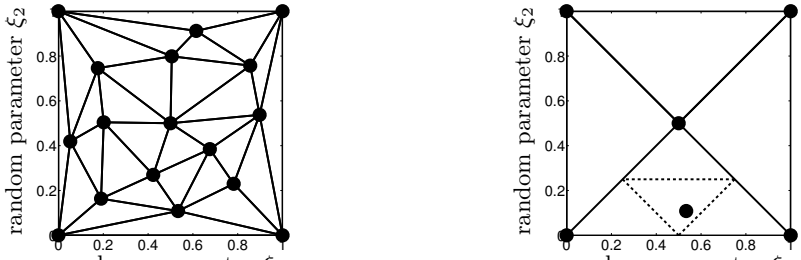

(a) $n_s = 17$ samples (b) Initial refinement

FIGURE 6. SSC discretization of a two-dimensional probability space with $n_\xi = 2$ aleatoric uncertain parameters ξ_1 and ξ_2, where the samples are represented by the filled circles.

not satisfied in the HyShot II problem. New methods that are able to treat correlated inputs given by a set of data points are therefore required.

3.2. *Simplex Stochastic Collocation*

In this section a Simplex Stochastic Collocation (SSC) method is introduced that discretizes the probability space using simplex elements (Witteveen *et al.* 2009; Witteveen & Iaccarino 2010*a*,*b*). An example of the SSC discretization is shown in Figure 6a for 2 aleatoric uncertainties and 17 samples. The two-dimensional probability space is divided into simplexes, or triangles in two dimensions, using a Delaunay triangulation of the sampling points. The approximation converges by adaptively refining the simplexes based on a refinement measure in each of the elements. The subdomains are refined by randomly adding a sampling point in the simplex with the highest value of the refinement measure. Random sampling is employed since it is an effective sampling strategy in multiple dimensions. The Delaunay algorithm is flexible enough for interpolating the random points. The new sample is confined in a subdomain of the simplex in order to ensure a sufficient spread of the samples, see Figure 6b.

This good spread of sampling points is necessary to build a higher-degree polynomial interpolation of the samples. The interpolation is constructed in a simplex by defining a stencil of sampling points in the vertices of neighboring elements. In that way, the multi-element nature of the method is employed for the interpolation by reusing the samples in the other elements. In Figure 7, three examples of stencils are given for increasing polynomial degree p and stencil size n. A piecewise linear interpolation with $p = 1$ uses only the vertices of the simplex. For higher-degree interpolations, samples of the neighboring elements are added to the stencil. These two-dimensional examples can be extended, and are implemented, for an arbitrary number of dimensions. Limiters for the local polynomial degree are used, in analogy to the limiters for deterministic finite volume methods, e.g., Extremum Diminishing (ED), Total Variation Diminishing (TVD), and Monotonicity Preserving (MP), in order to achieve a robustness for discontinuities, which is consistent with the discretization in physical space.

In mathematical terms, the objective of SSC is to compute the probability distribution and the statistical moments μ_{u_i} of a QOI, $u(\boldsymbol{\xi})$, subject to n_ξ random parameters $\boldsymbol{\xi} = \{\xi_1, \ldots, \xi_{n_\xi}\}$

$$\mu_{u_i} = \int_\Xi u(\boldsymbol{\xi})^i f_\xi(\boldsymbol{\xi}) \mathrm{d}\boldsymbol{\xi} = \sum_{j=1}^{n_e} \int_{\Xi_j} u(\boldsymbol{\xi})^i f_\xi(\boldsymbol{\xi}) \mathrm{d}\boldsymbol{\xi}, \tag{3.1}$$

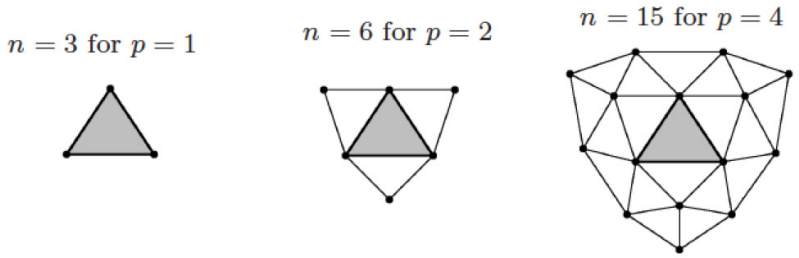

FIGURE 7. Two-dimensional higher-degree SSC interpolation stencils with polynomial degree p and stencil size n.

with

$$\boldsymbol{\xi} \in \Xi = \bigcup_{j=1}^{n_\mathrm{e}} \Xi_j, \tag{3.2}$$

where Ξ_j are n_e disjoint simplexes that cover the entire parameter space Ξ with $j = 1, \ldots, n_\mathrm{e}$. Since the exact response surface $u(\boldsymbol{\xi})$ in (3.1) is unknown, it is approximated by a piecewise polynomial interpolation $w(\boldsymbol{\xi})$ of n_s samples $\mathbf{v} = \{v_1, \ldots, v_{n_\mathrm{s}}\} = \{u(\boldsymbol{\xi}_1), \ldots, u(\boldsymbol{\xi}_{n_\mathrm{s}})\}$ with local polynomial degree p_j. A polynomial chaos-type expansion (Ghanem & Spanos 1991; Xiu & Karniadakis 2002) is used for the approximation $w_j(\boldsymbol{\xi})$ in the simplexes

$$u(\boldsymbol{\xi}) \approx w(\boldsymbol{\xi}) = w_j(\boldsymbol{\xi}) = \sum_{i=0}^{n_j} c_{ij} \Psi_{ij}(\boldsymbol{\xi}), \tag{3.3}$$

with $\boldsymbol{\xi} \in \Xi_j$ and basis polynomials $\Psi_{ij}(\boldsymbol{\xi})$ and coefficients c_{ij} for $i = 1, \ldots, n_j$ and $j = 1, \ldots, n_\mathrm{e}$. The number of terms in the expansion n_j is equal to

$$n_j + 1 = \frac{(n_\xi + p_j)!}{n_\xi! p_j!}. \tag{3.4}$$

The error convergence of the SSC method for an analytical test function is shown in Figure 8. The superlinear convergence of the randomized refinement sampling reduces the number of samples by up to two orders of magnitude, compared to using higher-degree Newton–Cotes quadrature points in the simplexes (see Figure 8a). The error estimate, compared to the exact error in Figure 8b, shows an accurate and slightly conservative approximation. The derivation of the error estimate is based on the hierarchical surplus, which is the difference between the sampled value v_k in a new sampling point $\boldsymbol{\xi}_k$ and the interpolated value $w(\boldsymbol{\xi}_k)$ at the previous approximation level. It represents the aleatoric uncertainty propagation error in the response surface approximation $w(\boldsymbol{\xi})$ with respect to the exact response $u(\boldsymbol{\xi})$ due to the finite number of samples $\mathbf{v}$. The availability of this estimate forms the basis of the framework for balancing uncertainties and errors.

4. Results

The SSC method is used to propagate aleatoric uncertainties in the flow conditions of the HyShot II flight experiment. This is combined with epistemic uncertainty in the choice of the RANS turbulence model. The numerical error is not considered in this study of HyShot II.

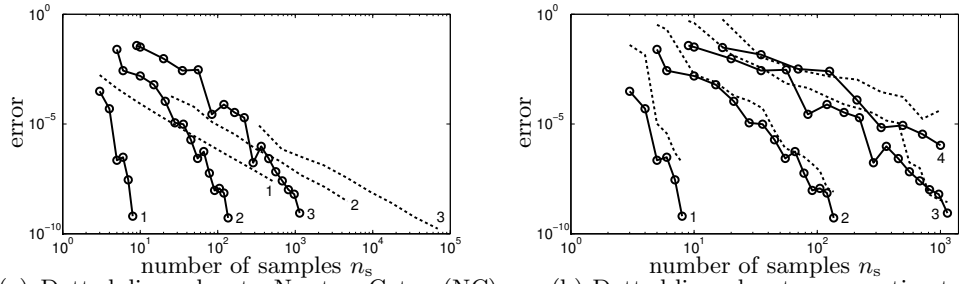

(a) Dotted lines denote Newton–Cotes (NC) sampling

(b) Dotted lines denote error estimate

FIGURE 8. SSC error convergence for an arctangent test function and $n_\xi = \{1, 2, 3, 4\}$ random parameters, where the continuous lines with circles denote the error for randomized refinement sampling.

4.1. *Aleatoric uncertainty quantification*

The SSC discretization of the aleatoric HyShot II flight conditions is shown in Figure 5b for $n_s = 11$ samples and $n_e = 16$ elements. The initial discretization consists of $n_e = 4$ triangular elements with samples at the four corners of the probability space and one in the center. The refined discretization leads to more samples in regions of higher probability in combination with a good spread of the sampling points for accurate interpolation. At $n_s = 11$ samples the first estimate of the aleatoric uncertainty propagation error is obtained. The result of Figure 5b shows that SSC is effective in discretizing the correlated inputs of the HyShot II case given by the MCMC data points.

The mean pressure field and standard deviation in the cold combustor are given in Figure 9 for the 11 aleatoric samples. These results are based on two-dimensional steady Reynolds Averaged Navier Stokes (RANS) simulations (Pečnik *et al.* 2009), with the Spalart-Allmaras turbulence model at constant specific heat ratio γ. The relative value of the energy residual is converged up to 10^{-4}. In the mean pressure field, the shock train in the combustor can be recognized. The standard deviation is highest near the shocks, particularly at the shock wave/boundary layer interactions (SWBLI) where the shock train reflects from the combustor walls. The magnitude of the standard deviation is approximately 1% of that of the mean pressure, compared to a 2.1% and 0.2% input CV for the angle of attack and the altitude, respectively.

Wall pressure at the transducer locations is shown in Figure 10 in terms of the predicted mean, and the 99% computational and experimental confidence intervals. Thus aleatoric uncertainty alone does not fully account for the discrepancy with the experiments or with the size of the experimental uncertainty bar.

4.2. *Epistemic uncertainty quantification*

In addition to aleatoric uncertainty in the flight conditions, epistemic uncertainty in the RANS turbulence model is also considered. An interval description can be used to represent model form uncertainty. There are several methodologies with increasing sophistication for computing epistemic uncertainty intervals. First, an epistemic uncertainty interval can be imposed on the QOI, as posteriori epistemic uncertainty quantification. A second approach is to propagate an epistemic uncertainty interval for an input parameter through the computational model. Another option is to inject epistemic uncertainty at selected regions in physical space based on a sensor approach.

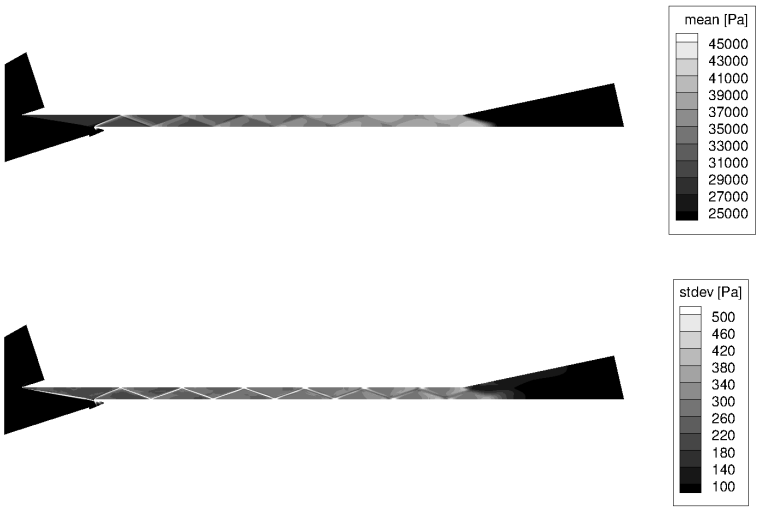

FIGURE 9. SSC results for the mean pressure and standard deviation fields for the cold HyShot II combustor with aleatoric flight conditions: Top figure denotes mean and bottom figure denotes standard deviation.

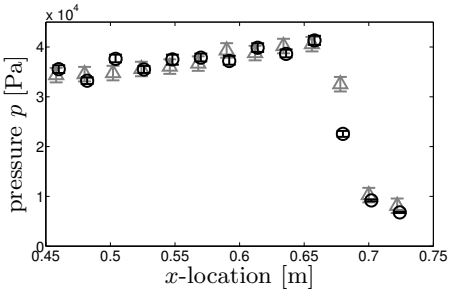

FIGURE 10. SSC results for the mean and 99% confidence intervals of the combustor wall pressure of the cold HyShot II combustor with aleatoric flight conditions compared to the experimental uncertainty bars: Black circles and bars denote predicted mean and confidence bar, and grey bars with triangles denote experimental results.

Posteriori epistemic uncertainty quantification is currently the only feasible option for quantifying the epistemic uncertainty related to the choice of the RANS turbulence model in the HyShot II simulation. In Figure 11, the results for the Spalart–Allmaras and Menter k–ω SST turbulence models are shown in terms of the wall pressure for the first aleatoric sample at $\alpha = 3.98^{\circ}$ and $h = 34.1$ km. The models lead to a significant difference in predicting of the pressure, with a maximum of 20% over all 11 aleatoric samples. The local difference between the minimum and maximum of the two predictions is used as the posteriori epistemic uncertainty interval for wall pressure. Since only two turbulence models are considered, the interval is an estimate of the minimum uncertainty involved with the choice of model. This is a first step to quantify epistemic uncertainty in the HyShot II case. The total epistemic uncertainty is larger since, for example, the effect of the RANS assumptions is not taken into account here. The non-reacting case is considered here to eliminate additional epistemic uncertainty stemming from mixing and combustion models.

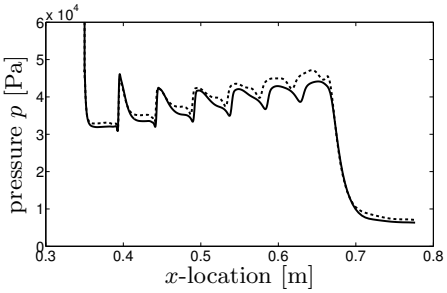

FIGURE 11. Epistemic uncertainty due to the choice of the RANS Spalart–Allmaras or Menter k–ω SST turbulence model for the first aleatoric sample of the cold HyShot II combustor: Continuous line denotes Spalart–Allmaras and dashed line denotes Menter k–ω SST turbulence model.

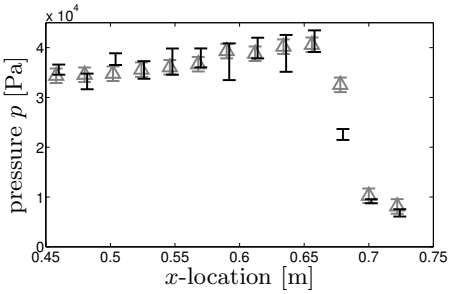

FIGURE 12. Mean and 99% confidence intervals of the combustor wall pressure of the cold HyShot II combustor with aleatoric flight conditions and epistemic RANS turbulence model compared to the experimental uncertainty bars: Black bars denote predicted confidence bar, and gray bars with triangles denote experimental results.

4.3. *Combination of aleatoric and epistemic uncertainty*

The prediction of wall pressure including the effect of both aleatoric and epistemic uncertainty is compared to the measurements in Figure 12 in terms of the 99% confidence intervals. The computational interval accounts for the aleatoric uncertainty, the aleatoric uncertainty propagation error, and epistemic uncertainty. The new predicted intervals show significant improvement over using only aleatoric uncertainty, in the sense that they overlap to a larger extent with the experiments.

The confidence bars are derived from the cumulative probability distribution functions (CDF). A example of such a CDF for the first pressure transducer is shown in Figure 13. Because of the combined effect of aleatoric and epistemic uncertainty, the probability distribution is also given in terms of a confidence band. The CDF accounts for the probabilistic character of aleatoric uncertainty, whereas the interval represents epistemic uncertainty and aleatoric propagation error. The 99% confidence bar of Figure 12 is then given by the 99% percentiles of the CDF, denoted by the circles in Figure 13.

We can now consider the balance of aleatoric and epistemic uncertainty, for example, for the approximation of the mean. The aleatoric uncertainty propagation error for $n_\mathrm{s} = 11$ samples of 15.9 Pa is negligible compared to the deterministic value of $3.5 \cdot 10^4$ Pa for the first pressure transducer, which is representative for the solution as a whole. In contrast, the effect of epistemic uncertainty in the RANS turbulence model is more than an order of magnitude larger with 224.1 Pa. The conclusion of the first step of the framework of Figure 4 is that the minimum of $n_\mathrm{s} = 11$ aleatoric samples is already sufficient in this

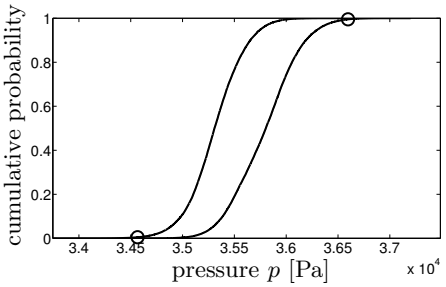

FIGURE 13. Confidence interval of the cumulative probability distribution function (CDF) for the first wall pressure transducer of the cold HyShot II combustor with aleatoric flight conditions and epistemic RANS turbulence model. The circles denote the 99% confidence percentiles.

case. If it is necessary to further improve the predictive capability of the simulation, this analysis points out that the epistemic uncertainty needs to be reduced. This reduction can be achieved by replacing the RANS computations by Large Eddy Simulations (LES) or by calibrating the RANS model using experimental data for the HyShot II case.

5. Future plans

A framework for balancing uncertainties and errors is presented and applied to the uncertainty quantification simulation of the HyShot II flight experiment. The aleatoric uncertainty propagation is performed using the Simplex Stochastic Collocation (SSC) method, which is effective in discretizing the correlated input given by a set of data points for the aleatoric flight conditions. It includes accurate error estimates for the aleatoric uncertainty propagation error, thereby forming the basis of the framework for balancing uncertainties and errors. Epistemic uncertainty quantification is performed for the choice of the RANS turbulence model by comparing the results of both the Spalart-Allmaras and the Menter k–ω SST models. A more comprehensive approach for the quantification of epistemic uncertainties in the HyShot II simulation is a point of ongoing research. The effect of numerical error will be included in the application of the framework to the HyShot II flight experiment in future work using error estimation based on an adjoint solver. This study is a preliminary analysis for the validation of the reactive case involving mixing and combustion physics. The perspective of this work is to use the presented framework for balancing uncertainties and errors on a routine basis in all full-system simulations and unit problem validations.

Acknowledgments

We would like to thank Alireza Doostan for providing the Bayesian inference results for the HyShot II flight conditions and Rene Pečnik for assisting with the deterministic HyShot II simulations. This work was supported by the United States Department of Energy under the Predictive Science Academic Alliance Program (PSAAP) at Stanford University, Award Number DE-FC52-08NA28614.

REFERENCES

BABUŠKA, I., NOBILE, F. & TEMPONE, R. 2007 A stochastic collocation method for

elliptic partial differential equations with random input data. *SIAM J. Numer. Anal.* **45**, 1005–1034.

Constantine, P. G., Doostan, A., Wang, Q. & Iaccarino, G. 2010 A surrogate accelerated Bayesian inverse analysis of the HyShot II supersonic combustion data. In *Proceedings of the Summer Program, Center for Turbulence Research, Stanford University*.

Ghanem, R. & Spanos, P. 1991 *Stochastic Finite Elements: A Spectral Approach*. Springer–Verlag, New York.

Jakeman, J., Eldred, M. & Xiu, D. 2010 Numerical approach for quantification of epistemic uncertainty. *J. Comput. Phys.* **229**, 4648–4663.

Oberkampf, W. L., Trucano, T. G. & Hirsch, C. 2004 Verification, validation, and predictive capability in computational engineering and physics. *Appl. Mech. Rev.* **57**, 345–384.

Pečnik, R., Terrapon, V., Ham, F. & Iaccarino, G. 2009 Full system scramjet simulation. In *Annual Research Briefs, Center for Turbulence Research, Stanford University*, pp. 33–45.

Smart, M., Hass, N. & Paull, A. 2006 Flight data analysis of the HyShot 2 scramjet flight experiment. *AIAA J.* **44**, 2366–2375.

Tang, G., Iaccarino, G. & Eldred, M. 2010 Using stochastic expansion methods in evidence theory for uncertainty quantification. In *Proceedings of the 12th AIAA Non-Deterministic Approaches Conference, Orlando, Florida*. AIAA-2010-2589.

Wang, Q., Duraisamy, K., Alonso, J. J. & Iaccarino, G. 2010 Risk assessment of scramjet unstart using adjoint-based sampling methods. In *Proceedings of the 12th AIAA Non-Deterministic Approaches Conference, Orlando, Florida*. AIAA-2010-2921.

Witteveen, J. A. S., Doostan, A., Pečnik, R. & Iaccarino, G. 2009 Uncertainty quantification of the transonic flow around the RAE 2822 airfoil. In *Annual Research Briefs, Center for Turbulence Research, Stanford University*.

Witteveen, J. A. S. & Iaccarino, G. 2010*a* Simplex elements stochastic collocation for uncertainty propagation in robust design optimization. In *Proceedings of the 48th AIAA Aerospace Sciences Meeting, Orlando, Florida*. AIAA-2010-1313.

Witteveen, J. A. S. & Iaccarino, G. 2010*b* Simplex elements stochastic collocation in higher-dimensional probability spaces. In *Proceedings of the 12th AIAA Non-Deterministic Approaches Conference, Orlando, Florida*. AIAA–2010–2924.

Xiu, D. & Hesthaven, J. S. 2005 High-order collocation methods for differential equations with random inputs. *SIAM J. Sci. Comput.* **27**, 1118–1139.

Xiu, D. & Karniadakis, G. E. 2002 The Wiener–Askey polynomial chaos for stochastic differential equations. *SIAM J. Sci. Comput.* **24**, 619–644.